Journal of Nuclear Medicine, published on August 21, 2020 as doi:10.2967/jnumed.120.246595

Noninvasive evaluation of CD20 expression using ^{64}Cu-labeled F(ab')$_2$ fragments of obinutuzumab in lymphoma

Lei Kang[1,2], Cuicui Li[1], Zachary T. Rosenkrans[3], Jonathan W. Engle[2], Rongfu Wang[1], Dawei Jiang[2,4], Xiaojie Xu[5], and Weibo Cai[2,3]

[1] Department of Nuclear Medicine, Peking University First Hospital, Beijing, China

[2] Departments of Radiology and Medical Physics, University of Wisconsin - Madison, WI, USA

[3] Department of Pharmaceutical Sciences, University of Wisconsin - Madison, Madison, WI, USA

[4] Department of Nuclear Medicine, Union Hospital, Tongji Medical College, Huazhong University of Science and Technology, Wuhan, China.

[5] Department of Medical Molecular Biology, Beijing Institute of Biotechnology, Beijing, China

Running Title: Imaging lymphoma with F(ab')$_2$ fragment

Lei Kang and Cuicui Li contributed equally to this work.

First Authors:

Lei Kang (MD, PhD), Cuicui Li (MD, PhD)

No.8, Xishiku St., West District, Beijing, 100034, China.

E-mail: kanglei@bjmu.edu.cn, licuicui199111@sina.com

Corresponding Authors:

Weibo Cai (PhD)

1111 Highland Avenue, Madison, WI 53705-2275, USA.

E-mail: wcai@uwhealth.org

Xiaojie Xu (PhD)

27 Taiping Rd, Beijing, 100850, China.

E-mail: miraclexxj@126.com

Dawei Jiang (PhD)

1277 Jiefang Avenue, Wuhan, Hubei 430022, China.

E-mail: dawei.jiang2020@outlook.com

Lei Kang (MD, PhD)

8 Xishiku Str., Xicheng Dist., Beijing, 100034, China.

E-mail: kanglei@bjmu.edu.cn

Word Count: 5276

ABSTRACT

CD20 over-expressed non-Hodgkin lymphoma typically shows progressive malignancy. Obinutuzumab (obi) is a next-generation FDA-approved humanized monoclonal antibody that targets CD20. Previous studies with ^{89}Zr-labeled obi has successfully imaged CD20 *in vivo*. However, delayed tumor uptake and increased radioactive exposure caused by long blood circulation limits its clinical translation. This study aims to develop ^{64}Cu-labeled F(ab')$_2$ fragments of obi for imaging CD20 in lymphoma xenograft tumor models. ***Methods*** F(ab')$_2$ fragments were produced from obi using an IdeS enzyme and purified with Protein A beads. SDS-PAGE and HPLC analysis were performed to evaluate the products and their stability. F(ab')$_2$ products were conjugated with p-SCN-Bn-NOTA (NOTA) for ^{64}Cu radiolabeling. Western blotting was performed to screen the CD20 expression levels of lymphoma cells. ELISA, flow cytometry and confocal imaging were used to test the binding affinity *in vitro*. Serial PET imaging and biodistribution studies in subcutaneous lymphoma-bearing mice were performed using ^{64}Cu-NOTA-F(ab')$_2$-obi or ^{64}Cu-NOTA-F(ab')$_2$-IgG. ***Results*** F(ab')$_2$-obi and F(ab')$_2$-IgG produced by the IdeS digestion system was confirmed with SDS-PAGE and HPLC analysis. The radiochemical purity of ^{64}Cu-labeled F(ab')$_2$ fragments was no less than 98% and the specific activity was 56.3 ± 7.9 MBq/mg (n=6). Among the five lymphoma cell lines, Ramos showed the strongest expression of CD20 and CLL-155 showed the lowest as confirmed by ELISA, flow cytometry, and confocal imaging. PET imaging revealed rapid and sustained tumor uptake of ^{64}Cu-NOTA-F(ab')$_2$-obi in Ramos tumor-bearing mice. The peak tumor uptake (9.08 ± 1.67 %ID/g) in Ramos model was significantly higher than that in the CCL-155 model (2.78 ± 0.62 %ID/g) or the ^{64}Cu-NOTA-F(ab')$_2$-IgG control (1.93 ± 0.26 %ID/g, n=4, P<0.001). The tumor-to-blood and tumor-to-muscle ratios were 7.3 ± 1.6 and 21.9 ± 9.0, respectively at 48 h p.i in the ^{64}Cu-NOTA-F(ab')$_2$-obi group. Of the measured off-target organs, the kidneys showed the highest uptake. *Ex vivo* immunofluorescent staining verified the differential CD20 expression in the Ramos and CCL-155 tumor models. ***Conclusions*** This study demonstrated that ^{64}Cu-NOTA-F(ab')$_2$-obi had a rapid and sustained tumor uptake in CD20-positive lymphoma with high contrast, which could enable noninvasive evaluation of CD20 levels in the clinic.

Keywords F(ab')$_2$; obinutuzumab; CD20; Positron emission tomography (PET); lymphoma

Introduction

Non-Hodgkin's lymphoma (NHL) is a class of heterogeneous lymphoid hematological malignancies primarily with B-cell origin (B-NHL, about 85%) (*1*). CD20 is highly expressed in malignant B cells, especially B-NHL, and is considered an important diagnosis biomarker and therapeutic target (*2*). Monoclonal antibodies (mAbs) targeting CD20 have high therapeutic efficacy in the clinic. Rituximab, a first generation CD20-targeted mAb, has saved millions of patients suffering from B-cell malignancies. However, this chimeric antibody may induce immunogenicity leading to treatment failure(*3*) Obinutuzumab (obi) is a next-generation humanized and glycoengineered type II IgG1 mAb targeting CD20. It recognizes a unique epitope and significantly increases the direct cell death compared to rituximab (*4*).

The expression of CD20 is a marker for evaluating the treatment efficacy. Although pathological results are the gold standard, acquiring samples is typically invasive and inconvenient. ^{18}F-fluorodeoxyglucose (^{18}F-FDG) PET/CT is currently the primary technique for therapeutic evaluation of lymphoma. However, ^{18}F-FDG is a non-specific agent which complicates diagnosis and may create false results. ImmunoPET is a non-invasive molecular imaging method that utilizes a radiolabeled antibody (*5,6*) to visualize a specific marker. This was previously demonstrated with ^{89}Zr-labeled obi that successfully assessed CD20 expression in murine tumor models (*7*).

Fab (~50 kDa) and F(ab')$_2$ (~110 kDa) fragments from an IgG antibody (~150 kDa) can be produced by enzymatic digestion, and they retain the same antigen-binding site and immunological binding activity as the intact antibody (*8*). Imaging agents based on intact antibodies are frequently limited by their long circulation half-life in the body and slow tumor penetration leading to delayed peak tumor uptake at several

days post-injection (p.i.) (*5*). In our previous study, immunoPET imaging with a ^{89}Zr-labeled CD38-targeted mAb (daratumumab) exhibited a specific binding ability for delineating lymphoma tumors *in vivo* (*9*). However, the tumor uptake peaked at 5 days p.i. and the radioactivity in the blood remained high up to four days. Since F(ab')$_2$ fragments are eliminated from blood more rapidly compared to intact mAbs while retaining high binding affinity(*8,10*), it may be propitious to prepare F(ab')$_2$ fragments of obi for PET imaging of lymphoma. In this study, we aim to develop F(ab')$_2$-obi for immunoPET imaging of CD20 in lymphoma murine models with a shortened imaging window.

Materials and methods

Preparation of F(ab')$_2$ fragments

F(ab')$_2$-obi were prepared using the IdeS protease kit (Promega) and purified by removing the Fc portion. In brief, obi (Roche) was incubated with IdeS protease for 30 min at 37 °C in the digestion buffer (50 mM sodium phosphate, 150 mM NaCl, pH 6.6). The digested products were then incubated with Magne™ Protein A beads (Promega) for 1 h and centrifuged. The Fc portion attached to the beads were removed in the sediment while the purified F(ab')$_2$ stayed in the supernatant. The products were evaluated by sodium dodecyl sulfate polyacrylamide gel electrophoresis (SDS-PAGE) and high-performance liquid chromatography (HPLC). SDS-PAGE was conducted on a 12% gel under 120 V for 1 h. The non-reducing gel was stained by Coomassie brilliant blue at room temperature (RT). HPLC was performed on a Dionex UltiMate3000 Chromeleon system (ThermoFisher). F(ab')$_2$ of a isotype IgG (ThermoFisher) were prepared as a control.

Stability test

$F(ab')_2$-obi (4.58 μM) was incubated in PBS or 10% of fetal bovine serum (FBS, Invitrogen) at 37 °C for 2, 4, 6, 12, and 24 h, respectively. The solvents were analyzed by SDS-PAGE using the same condition described above.

Radiolabeling

$F(ab')_2$-obi was labeled by ^{64}Cu ($t_{1/2}$ = 12.7 h) after conjugated with 1,4,7-triazacyclononane-1,4,7-triacetic acid (NOTA, Macrocyclics). In brief, $F(ab')_2$-obi was incubated with NOTA for 2 h at RT in a carbonate buffer (pH 9.0) and the molar ratio of $F(ab')_2$-to-NOTA was 1:10-20. NOTA-$F(ab')_2$-obi was purified using PD-10 columns (GE Healthcare) with PBS as the mobile phase. For radiolabeling with ^{64}Cu, NOTA-$F(ab')_2$-obi was incubated with $^{64}CuCl_2$ in sodium acetate buffer (pH 5.5) for 1 h at 37 °C and purified with PD-10 columns. The ratio of NOTA-$F(ab')_2$-to-$^{64}CuCl_2$ was no less than 0.68 μg/MBq. The similar protocol was used to prepare ^{64}Cu-labeled $F(ab')_2$-IgG.

Cell culture and xenograft model

Five lymphoma cell-lines including Ramos, Daudi, OCI-LY10, Raji, and CCL-155 were purchased from American Type Culture Collection. Cells were cultured in RPMI 1640 medium supplemented with 10% FBS and 1% penicillin/streptomycin (Invitrogen) at 37 °C with 5% CO_2.

Animal studies were approved by the Wisconsin University Institutional Animal Care and Use Committee. Immunodeficient male CB-17 SCID mice (4-6 weeks old, Envigo) were used to establish xenograft tumor models with Ramos and CCL-155 cells. Each mouse was subcutaneously injected with 1

× 10^7 of cells suspended in 200 µL Matrigel (Invitrogen) on its lower right flank. Health conditions and tumor volumes were monitored every other day.

Western blot

Western blot was used to screen the cellular CD20 expression. Collected proteins were loaded into the 4 - 12% Bolt Bis-Tris Plus gel (ThermoFisher), electrophorized for 60 min under 110 V at 4 °C and transferred to a nitrocellulose membrane. The membrane was blocked with Odyssey blocking buffer (LI-COR) at RT for 1 h and incubated with mouse anti-human CD20 (1:1000) and rabbit anti-human β-actin (1:2000) primary antibodies (Novus Biologicals) overnight at 4 °C. After washing with PBS-T (PBS with Tween 20), the membrane was incubated with donkey anti-mouse IRDye 800CW and goat anti-rabbit IRDye 680RD secondary antibodies (LI-COR) for scanning and analysis using Odyssey infrared imaging system (LI-COR).

Immunofluorescence cell staining

NHS-Fluorescein (NHS-FITC, ThermoFisher) was conjugated with $F(ab')_2$ at a molar ratio of 1:3 in a carbonate buffer (pH 9.0) for 2 h. The fluorescent product was purified using PD-10 columns by removing excess dye. When Ramos cells were cultured in 6-well plates at a confluence of 40%, FITC-$F(ab')_2$ were incubated at 10 ng/mL overnight. Cells were then collected and treated with DAPI-containing hard mount medium (Vector Laboratories). Imaging was performed using a Nikon confocal system (A1RS).

Flow cytometry

Ramos and CCL-155 cells were incubated with $F(ab')_2$-obi, obi, and IgG (10 µg/mL) in flow cytometry staining buffer solution (eBioscience) at 1 x 10^6 cells/mL for 30 min at RT. Cells were washed with cold

PBS (pH 7.4) and then incubated with a FITC-labeled goat anti-human IgG $F(ab')_2$ secondary antibody (3 μg/mL, ThermoFisher) for 20 min at RT. After washing, cells were analyzed using a FACSCanto II analyzer (BD Biosciences). Fluorescein intensities were processed with FlowJo software (Tree Star).

ELISA assay

In-cell indirect ELISA assay was used to test the binding affinity of $F(ab')_2$ in Ramos and CCL-155 cells. Obi and non-specific IgG were used as controls. In brief, various concentration of antibodies (0 - 134 nmol/L) were incubated with 1×10^5 cells for 1 h at RT in a 96-well culture plate (n=3). Cells were centrifuged at 1,650 rpm for 5 min and washed with cold PBS. A horseradish peroxidase (HRP)-coupled anti-human IgG $F(ab')_2$ secondary antibody (Abcam) was incubated (1:5000) for 30 min at RT. After washing, a peroxidase substrate (Abcam) was added, then stopped by equal volume of H_2SO_4 solution (2 M). Spectrophotometric readings were made at 450 nm using a Synergy H1 reader (BioTek). Maximum binding ability (B_{max}) and affinity constant (K_D) values were calculated using GraphPad Prism software (La Jolla).

PET imaging

PET imaging was performed when the diameter of tumors reached about 10 mm. Tumor-bearing mice were intravenously injected with 5 - 10 MBq of ^{64}Cu-labeled $F(ab')_2$-obi or $F(ab')_2$-IgG. After being anesthetized with 2% isoflurane, mice were imaged on an Inveon micro-PET/CT scanner (Siemens) at 10 min, 4 h, 12 h, 24 h, and 48 h p.i. Twenty million coincidence events were collected at each time per mouse and images were reconstructed using a 3D workstation. Regions-of-interest (ROI) for the tumor, heart, liver, kidneys, bone and muscle were quantified with the Inveon Research Workspace (IRW) software.

Biodistribution

After terminal imaging time point, mice were euthanized by carbon dioxide asphyxiation. Major organs/tissues including the tumor, heart, liver, spleen, lung, kidneys, stomach, intestine, pancreas, tail, skin, muscle, bone, brain, and blood were harvested, weighed, then activity was measured with an automated gamma counter (PerkinElmer). The biodistribution data was presented as percentage of injected dose per gram of tissue (%ID/g).

Immunofluorescence tissue staining

Immunofluorescence staining was performed following established protocols (*9,11,12*). After blocked with 10% donkey serum for 60 min, tissue slides were incubated with rabbit anti-human anti-CD20 (1:400, Novus Biologicals) and rat anti-mouse anti-CD31 (1:100, ThermoFisher) primary antibodies overnight at 4 ^{o}C. The slides were washed and stained with AlexaFluor488-labeled goat anti-rabbit and Cy3-labeled donkey anti-rat secondary antibodies (ThermoFisher). Slides were mounted with DAPI-containing hard mount medium and imaged with a Nikon A1RS confocal microscope.

Statistical analysis

All quantitative data was presented as mean ± standard deviation. Student's *t*-test was used for comparisons between groups. *P* values less than 0.05 were considered statistically significant.

Results

Preparation of ^{64}Cu-labeled F(ab')$_2$

F(ab')$_2$ were prepared by digesting intact mAbs using IdeS protease and purified with magnetic beads (**Fig.1a**). SDS-PAGE showed the molecular weight of obi was ~150 kDa while F(ab')$_2$-obi was ~100 kDa, consistent with the theoretical molecular weight (**Fig. 1b**). HPLC showed one main peak of F(ab')$_2$-obi locating after the obi peak (**Fig. 1c**), indicating that F(ab')$_2$-obi was successfully prepared with high purity. ^{64}Cu-labeled F(ab')$_2$-obi achieved a yield of more than 90% (n=6). Purified ^{64}Cu-NOTA-F(ab')$_2$-obi had a radiochemical purity of more than 98% and a specific activity of 56.3 ± 7.9 MBq/mg. SDS-PAGE showed that the bands of F(ab')$_2$-obi were clearly seen without diffusion over 24 h in PBS or 10% FBS, indicating excellent *in vitro* stability **(Fig. 1d)**.

Cellular screening and binding affinity

In western blot, Ramos showed the highest expression of CD20 while CLL-155 showed the lowest (**Fig. 2a**). Visualized by a confocal microscope, strong binding from FITC-F(ab')$_2$-obi was found on Ramos cells. In contrast, non-specific signal was observed for FITC-F(ab')$_2$-IgG or FITC dye only (**Fig. 2b**). Flow cytometry showed a strong signal shift after incubating F(ab')$_2$-obi and obi with Ramos cells, suggesting the specific binding of F(ab')$_2$-obi and obi with CD20 (**Fig. 2c**). Cell binding results from ELISA assay indicated that F(ab')$_2$-obi and obi had high binding affinity with Ramos cells but only nonspecific binding with CCL-155 cells. The K_D value of F(ab')$_2$-obi and obi is 3.7 ± 0.6 nM and 1.5 ± 0.4 nM while their B_{max} values are both 0.22 ± 0.01 pmol and the receptor density of Ramos cells is ~1.33 ×10^6 per cell (**Fig. 2d**).

PET imaging and quantitative analysis

The maximum intensity projection (MIP) images of ^{64}Cu-NOTA-F(ab')$_2$-obi and ^{64}Cu-NOTA-F(ab')$_2$-IgG are displayed in **Fig. 3**. Ramos tumor showed high tracer uptake and excellent contrast as early as 4 h and peaked at 12 h p.i. of ^{64}Cu-NOTA-F(ab')$_2$-obi. In contrast, ^{64}Cu-NOTA-F(ab')$_2$-IgG could not delineate the tumor at any time point. CCL-155 tumors showed a near-uniform tumor-to-background uptake of ^{64}Cu-NOTA-F(ab')$_2$-obi. Both F(ab')$_2$-obi and F(ab')$_2$-IgG had high uptake in kidneys and bladder due to the clearance via urinary system. Tracer uptake in large blood vessels and blood-rich organs decreased significantly after 4 h, suggesting F(ab')$_2$ had an optimal *in vivo* blood clearance.

Quantitative ROI analysis (**Fig. 4a**) observed high and sustained tumor uptake (> 7 %ID/g) for ^{64}Cu-NOTA-F(ab')$_2$-obi in the Ramos model. The highest tumor uptake of ^{64}Cu-NOTA-F(ab')$_2$-obi (9.08 ± 1.67 %ID/g) occurred at 12 h p.i. in the Ramos model, which was significantly higher than CCL-155 (2.78 ± 0.62 %ID/g, P=0.000001, n=4). In comparison, the peak tumor uptake of ^{64}Cu-NOTA-F(ab')$_2$-IgG was significantly lower than that of ^{64}Cu-NOTA-F(ab')$_2$-obi (P=0.000001) with only 1.93 ± 0.26 %ID/g (n=4). In all three groups, the radioactive uptake of kidneys reached a maximum between 4 and 12 h and then decreased. The uptake in other organs (heart, liver, bone, and muscle) was highest immediately after injection and then decreased over time. Tumor-to-blood (T/B) and tumor-to-muscle (T/M) ratios (**Fig. 4b**) increased gradually and peaked at 7.32 ± 1.61 and 21.88 ± 8.99 at 48 h p.i. of ^{64}Cu-NOTA-F(ab')$_2$-obi in the Ramos model. The highest T/B ratios of the F(ab')$_2$-IgG group (1.09 ± 0.33) and CCL-155 group (1.50 ± 0.48) were significantly lower (P=0.000002 and 0.000004). These quantitative results indicated that ^{64}Cu-NOTA-F(ab')$_2$-obi could specifically visualize differential expression of CD20 *in vivo*.

***Ex vivo* biodistribution**

Overall, the biodistribution results at 48 h (n=4) corroborated the above ROI analysis (**Fig. 5**). The tumor uptake of $F(ab')_2$-obi in Ramos (6.07 ± 0.57 %ID/g) was significantly higher than in CCL-155 (1.14 ± 0.21 %ID/g, P=0.000001) and $F(ab')_2$-IgG in Ramos (0.80 ± 0.18 %ID/g, P=0.000001). Renal uptake in three groups (15.32 ± 0.88, 14.34 ± 1.03, and 12.36 ± 3.19 %ID/g) was not statistically different ($P>0.05$). Blood retention of $F(ab')_2$-obi in the Ramos model (0.45 ± 0.11 %ID/g) was lower than other groups (0.76 ± 0.10 and 0.86 ± 0.09 %ID/g, P=0.03 and 0.02), probably due to higher tumor uptake. The biodistribution of all other organs/tissues showed no statistical difference ($P>0.05$).

Tumor tissues staining

Ramos and CCL-155 tumors were removed and stained for CD20 expression (**Fig.6**). Ramos tumor showed strong CD20 signal (green) around the cell membrane in tumors while CCL-155 showed very weak signal, which correlated well with PET observation. CD31 staining indicated rich angiogenesis in both tumors.

Discussion

CD20 is overexpressed in 90% of B-cell lymphomas, which account for about 85% of all lymphomas. 20-40% of HL is also CD20-positive (*7*). The evaluation of CD20 expression is important to assess treatment efficacy. While rituximab, a first generation anti-CD20 mAb, has long been publicly recognized for its therapeutic efficacy in lymphoma, its potential as a specific imaging agent targeting CD20 has only recently been investigated (*13,14*). Obi is the first type II, glycoengineered anti-CD20 humanized mAb. Compared to rituximab, obi is less immunogenic, more effective at inducing direct cell death, and has a higher binding affinity (*15*). Due to these advantages, obi would be a better choice for CD20-specific immunoPET imaging.

ImmunoPET combines the specificity of antibodies with the sensitivity of PET imaging, facilitating noninvasive evaluation of unique phenotypes of tumors *in vivo* (*6,16*). Large size of intact antibodies (~150 kDa) potentially hinders the clinical translation of antibody-based imaging agents for several reasons. First, delayed peak tumor uptake at days after administration limits the possibility of imaging on the same day of injection. In previous studies, ^{89}Zr-labeled rituximab or obi required up to 7 days to reach maximal uptake in CD20-positive animal models (*7,13*). When ^{89}Zr-labeled rituximab was used in patients with diffuse large B cell lymphoma, its optimal tumor uptake was also at 6 d p.i. (*14*). Second, intact antibodies have slow blood clearance and relatively high uptake in the liver from hepatic clearance. These characteristics decrease the target contrast and worsen imaging quality. Third, studying the long-term biodistribution of intact antibodies requires radionuclides with longer half-lives, such as ^{89}Zr ($t_{1/2}$ = 78.4 h) and ^{124}I ($t_{1/2}$ = 100.8 h). This will typically expose patients more radiation (*17*). Due to these disadvantages, alternative immunoPET imaging probes must be developed for successful clinical translation.

$F(ab')_2$ fragments, lacking the Fc portion of mAbs, have shorter blood circulation and interact less with complements compared to intact mAbs (*18*). According to a previous study, the highest tumor uptake (44.4 ±7.6 %ID/g) of ^{89}Zr-obi in Raji tumors (CD20-positive) occurred at 7 d (*7*). In our study, the highest ^{64}Cu-NOTA-$F(ab')_2$-obi tumor uptake (9.1±1.7 %ID/g) occurred at 12 h p.i. in the Ramos model, which was much earlier compared to ^{89}Zr-obi. By comparing the cellular binding affinity of $F(ab')_2$-obi and obi, our study found that they had specific binding with Ramos cells with similar Bmax (0.22 ± 0.01 pmol) and high K_D values (< 4 nM). Importantly, our study found similar tumor uptake (8.3 ± 2.0 %ID/g) can be obtained at a time point as early as 4 h p.i. of ^{64}Cu-NOTA-$F(ab')_2$-obi. The rapid and prominent tumor uptake makes ^{64}Cu-NOTA-$F(ab')_2$-obi suitable for clinical translation by enabling same-day imaging and improving the imaging quality compared to the intact mAb. Compared to F(ab), $F(ab')_2$ typically has a longer circulation half-life and higher tumor uptake. Mendler et al (*19*) prepared a ^{125}I-labeled Fab of ofatumumab that is a full human CD20 mAb, but found that tumor uptake was low (1.3 ± 0.1 %ID/g at 6 h and 0.2 %ID/g at 24h). Our results suggested $F(ab')_2$ may be a better choice for tumor imaging compared to F(ab). ^{64}Cu has a half-life of 12.7 h and is an excellent match with the time required for peak tumor uptake in this study.

Another advantage of $F(ab')_2$ for imaging is the better tumor contrast stemming from faster blood clearance (*20*). In our study, the T/B ratio reached 7.3 ± 1.6 at 2 d. In comparison, the same T/B ratio was obtained 7 d p.i of ^{89}Zr-obi (*7*). Compared to ^{89}Zr-rituximab, ^{64}Cu-NOTA-$F(ab')_2$-obi achieved a high T/M ratio (21.9 ± 9.0) at 5 d earlier at 2 d p.i. (*13*). Moreover, both ^{64}Cu-NOTA-$F(ab')_2$-obi in CCL-155 tumors and ^{64}Cu-NOTA-$F(ab')_2$-IgG in Ramos tumors showed significantly lower tumor contrast at 48 h p.i. (T/B = 1.5 ± 0.5 and 1.1 ± 0.3; T/M = 7.9 ± 4.0 and 4.6 ± 2.4, respectively). Although ^{68}Ga-labeled F(ab) and $F(ab')_2$

of rituximab have been previously developed, they were only evaluated at the cellular level (*21*). Therefore, our study confirms that ^{64}Cu-labeled F(ab')$_2$-obi is promising to evaluate the differential CD20 expression of lymphoma noninvasively.

A concise understanding of the properties of ^{64}Cu-labeled F(ab')$_2$-obi will guide the future application and clinical translation to ensure its *in vivo* performance. Generally, favorable radiolabeling efficiency, high specific activity, and good stability are essential (*6*). Cooper et al (*22*) compared the labeling, *in vitro*, *in vivo* characteristics of eight commonly used chelators for ^{64}Cu-radiolabeling and concluded that NOTA had significant advantages over other tested chelators. NOTA-chelated rituximab could be radiolabeled rapidly at RT with high serum stability for over 48 h. To provide homogenous, uniform and predictable products, site-specific conjugation methods have been used in the preparation of radiolabeled antibodies, via the modification of endogenous sites on antibodies (*23*), addition of cysteine residues (*5,24*) and some click chemistry pairs (*25*).

To image CD20 *in vivo*, some antibody-derived imaging probes with smaller sizes have been developed. Olafsen et al (*26*) developed a 80 kDa minibody and a modified scFv-Fc (105 kDa) from rituximab. The ^{124}I-minibody reached at maximum tumor uptake of 12.9 ± 3.4 %ID/g at 21 h p.i. in a CD20-positive lymphoma murine model. The T/B ratio was only 4.8 ± 1.5, which is significantly lower than F(ab')$_2$-obi in our study. Krasniqi et al (*27*) developed camelid single domain Ab fragments (sdAbs) with a very small size (<15 kDa). The T/B ratio was also drastically lower than our study but was acceptable (3.7 ± 0.7) at 1.5 h p.i. of ^{68}Ga-NOTA-sdAb. However, the tumor uptake was only 3.4 ± 1.3 %ID/g and decreased to 1.6 ± 0.1 %ID/g at 6 h p.i. Another immunoPET study used ^{89}Zr- or ^{124}I-labeled cysteine-diabodies derived

from obi and found that ^{89}Zr-cys-diabody yielded greater tumor uptake (4.9 ± 0.3 %ID/g at 24 h) and T/B ratio (14.4 ± 1.5 at 24 h) compared with ^{124}I-labeled tracers (*24*). In our study, ^{64}Cu-labeled F(ab')$_2$ is also bivalent and features the residualizing PET isotope. Compared with ^{89}Zr-cys-diabody, the tumor uptake of F(ab')$_2$ showed a comparable level (8.3 ± 1.9 %ID/g vs ~9 %ID/g) at 4 h but a higher level (7.4 ± 1.4 %ID/g vs 4.9 ± 0.3 %ID/g) at 24 h, while the T/B ratio at 24 h was less (5.2 ± 2.2 vs 14.4 ± 1.5). Since their K_D values are in the similar low nanomolar range of less than 4 nM, the difference of tumor uptake might be relative with the larger size of F(ab')$_2$ and the different CD20 level of Ramos. Because of the residualizing nature of ^{89}Zr, ^{89}Zr-cys-diabody showed higher nonspecific uptake, especially in the kidneys than ^{124}I-labeled tracer. Although ^{64}Cu-labeled F(ab')$_2$ showed high non-target uptake in the kidneys (21.0 ± 7.8 %ID/g at 24 h), it is much lower than ^{89}Zr-cys-diabody (106.8 ± 2.5 %ID/g at 24 h), suggesting better contrast of the kidneys.

Although antibody fragments can significantly enhance blood clearance and tumor contrast, these small tracers typically undergo rapid renal filtration and elimination (*16*). Radiolabeled agents of similar or smaller size would have also high renal uptake (*21*). These lead to high kidney accumulation and may induce nephrotoxicity. Some strategies have been used to reduce renal uptake. The conjugation of polyethylene glycol (PEG) to antibody fragments was used to increase the molecular weight beyond the cut-off for glomerular filtration, but increased circulation half-life (*28*). A pre-targeting strategy separately administering the antibody-based probe and the radionuclide have also been used to decrease renal radionuclide accumulation (*29*). However, pre-targeting requires optimization which makes it difficult and

also typically reduces tumor uptake. Therefore, the optimal size of mAb fragments using feasible methods requires further investigation in the future.

Conclusion

This study used a ^{64}Cu-labeled F(ab')$_2$ of obi to visualize the differential expression of CD20 *in vivo*. ^{64}Cu-NOTA-F(ab')$_2$-obi was found to be a specific and efficient imaging agent for CD20-positive tumors. Furthermore, ^{64}Cu-NOTA-F(ab')$_2$-obi showed rapid and persistent tumor uptake with low background, which may allow for a same-day immunoPET imaging in future clinical application.

Conflict of Interest: The authors declare that they have no conflict of interest.

Ethical approval: All applicable international, national, and/or institutional guidelines for the care and use of animals were followed.

Acknowledgments:

This work was supported by the University of Wisconsin - Madison, the National Institutes of Health (P30CA014520), the National Natural Science Foundation of China (81871385), PKU medicine-X Youth Program (PKU2020LCXQ007) and Open Funding Project of the State Key Laboratory of Biochemical Engineering (2020KF-01).

KEY POINTS:

Question: Whether $F(ab')_2$ produced from Obinutuzumab can be used to accurately visualize differentiated CD20 expression of lymphoma.

Pertinent Findings: This work successfully produced ^{64}Cu-NOTA-$F(ab')_2$-obi and immunoPET imaging validated it as a specific and efficient tracer for CD20-positive tumors with excellent tumor contrast.

Implications for Patient Care: As a useful tool to characterize the dynamics of CD20-positive lymphoma, immunoPET imaging using anti-CD20 $F(ab')_2$ fragments can help refine clinical cancer diagnosis where $F(ab')_2$ tracers can be highly useful as efficacious same-day imaging tracers in the clinical setting.

References

1. Swerdlow SH, Campo E, Pileri SA, et al. The 2016 revision of the world health organization classification of lymphoid neoplasms. *Blood.* 2016;127:2375-2390.

2. Shanehbandi D, Majidi J, Kazemi T, Baradaran B, Aghebati-Maleki L. Cd20-based immunotherapy of b-cell derived hematologic malignancies. *Curr Cancer Drug Targets.* 2017;17:423-444.

3. Freeman CL, Sehn LH. A tale of two antibodies: Obinutuzumab versus rituximab. *Br J Haematol.* 2018;182:29-45.

4. Illidge T, Klein C, Sehn LH, Davies A, Salles G, Cartron G. Obinutuzumab in hematologic malignancies: Lessons learned to date. *Cancer Treat Rev.* 2015;41:784-792.

5. Zettlitz KA, Tavare R, Tsai WK, et al. (18)f-labeled anti-human cd20 cys-diabody for same-day immunopet in a model of aggressive b cell lymphoma in human cd20 transgenic mice. *Eur J Nucl Med Mol Imaging.* 2019;46:489-500.

6. Wei W, Rosenkrans ZT, Liu J, Huang G, Luo QY, Cai W. Immunopet: Concept, design, and applications. *Chem Rev.* 2020;120:3787-3851.

7. Yoon JT, Longtine MS, Marquez-Nostra BV, Wahl RL. Evaluation of next-generation anti-cd20 antibodies labeled with (89)zr in human lymphoma xenografts. *J Nucl Med.* 2018;59:1219-1224.

8. Hong H, Zhang Y, Orbay H, et al. Positron emission tomography imaging of tumor angiogenesis with a (61/64)cu-labeled f(ab')(2) antibody fragment. *Mol Pharm.* 2013;10:709-716.

9. Kang L, Jiang D, England CG, et al. Immunopet imaging of cd38 in murine lymphoma models using (89)zr-labeled daratumumab. *Eur J Nucl Med Mol Imaging.* 2018;45:1372-1381.

10. Luo H, Hernandez R, Hong H, et al. Noninvasive brain cancer imaging with a bispecific antibody fragment, generated via click chemistry. *Proc Natl Acad Sci U S A.* 2015;112:12806-12811.

11. England CG, Ehlerding EB, Hernandez R, et al. Preclinical pharmacokinetics and biodistribution studies of 89zr-labeled pembrolizumab. *J Nucl Med.* 2017;58:162-168.

12. Li S, England CG, Ehlerding EB, et al. Immunopet imaging of cd38 expression in hepatocellular carcinoma using (64)cu-labeled daratumumab. *Am J Transl Res.* 2019;11:6007-6015.

13. Natarajan A, Habte F, Gambhir SS. Development of a novel long-lived immunopet tracer for monitoring lymphoma therapy in a humanized transgenic mouse model. *Bioconjug Chem.* 2012;23:1221-1229.

14. Jauw YW, Zijlstra JM, de Jong D, et al. Performance of 89zr-labeled-rituximab-pet as an imaging biomarker to assess cd20 targeting: A pilot study in patients with relapsed/refractory diffuse large b cell lymphoma. *PLoS One.* 2017;12:e0169828.

15. Mossner E, Brunker P, Moser S, et al. Increasing the efficacy of cd20 antibody therapy through the engineering of a new type ii anti-cd20 antibody with enhanced direct and immune effector cell-mediated b-cell cytotoxicity. *Blood.* 2010;115:4393-4402.

16. England CG, Rui L, Cai W. Lymphoma: Current status of clinical and preclinical imaging with radiolabeled antibodies. *Eur J Nucl Med Mol Imaging.* 2017;44:517-532.

17. Cai W, Hong H, Zhang Y. Pet tracers based on zirconium-89. *Curr Radiopharm.* 2011;4:131-139.

18. Valedkarimi Z, Nasiri H, Aghebati-Maleki L, Abdolalizadeh J, Esparvarinha M, Majidi J. Production and characterization of anti-human igg f(ab')2 antibody fragment. *Hum Antibodies.* 2018;26:171-176.

19. Mendler CT, Friedrich L, Laitinen I, et al. High contrast tumor imaging with radio-labeled antibody fab fragments tailored for optimized pharmacokinetics via pasylation. *MAbs.* 2015;7:96-109.

20. Fu R, Carroll L, Yahioglu G, Aboagye EO, Miller PW. Antibody fragment and affibody immunopet imaging agents: Radiolabelling strategies and applications. *ChemMedChem.* 2018;13:2466-2478.

21. Suman SK, Kameswaran M, Pandey U, Sarma HD, Dash A. Preparation and preliminary bioevaluation studies of (68) ga-nota-rituximab fragments as radioimmunoscintigraphic agents for non-hodgkin lymphoma. *J Labelled Comp Radiopharm.* 2019;62:850-859.

22. Cooper MS, Ma MT, Sunassee K, et al. Comparison of (64)cu-complexing bifunctional chelators for radioimmunoconjugation: Labeling efficiency, specific activity, and in vitro/in vivo stability. *Bioconjug Chem.* 2012;23:1029-1039.

23. Wu AM. Engineered antibodies for molecular imaging of cancer. *Methods.* 2014;65:139-147.

24. Zettlitz KA, Tavare R, Knowles SM, Steward KK, Timmerman JM, Wu AM. Immunopet of malignant and normal b cells with (89)zr- and (124)i-labeled obinutuzumab antibody fragments reveals differential cd20 internalization in vivo. *Clin Cancer Res.* 2017;23:7242-7252.

25. Morais M, Ma MT. Site-specific chelator-antibody conjugation for pet and spect imaging with radiometals. *Drug Discov Today Technol.* 2018;30:91-104.

26. Olafsen T, Betting D, Kenanova VE, et al. Recombinant anti-cd20 antibody fragments for small-animal pet imaging of b-cell lymphomas. *J Nucl Med.* 2009;50:1500-1508.

27. Krasniqi A, D'Huyvetter M, Xavier C, et al. Theranostic radiolabeled anti-cd20 sdab for targeted radionuclide therapy of non-hodgkin lymphoma. *Mol Cancer Ther.* 2017;16:2828-2839.

28. Li L, Turatti F, Crow D, et al. Monodispersed dota-peg-conjugated anti-tag-72 diabody has low kidney uptake and high tumor-to-blood ratios resulting in improved 64cu pet. *J Nucl Med.* 2010;51:1139-1146.

29. van Duijnhoven SM, Rossin R, van den Bosch SM, Wheatcroft MP, Hudson PJ, Robillard MS. Diabody pretargeting with click chemistry in vivo. *J Nucl Med.* 2015;56:1422-1428.

Figures

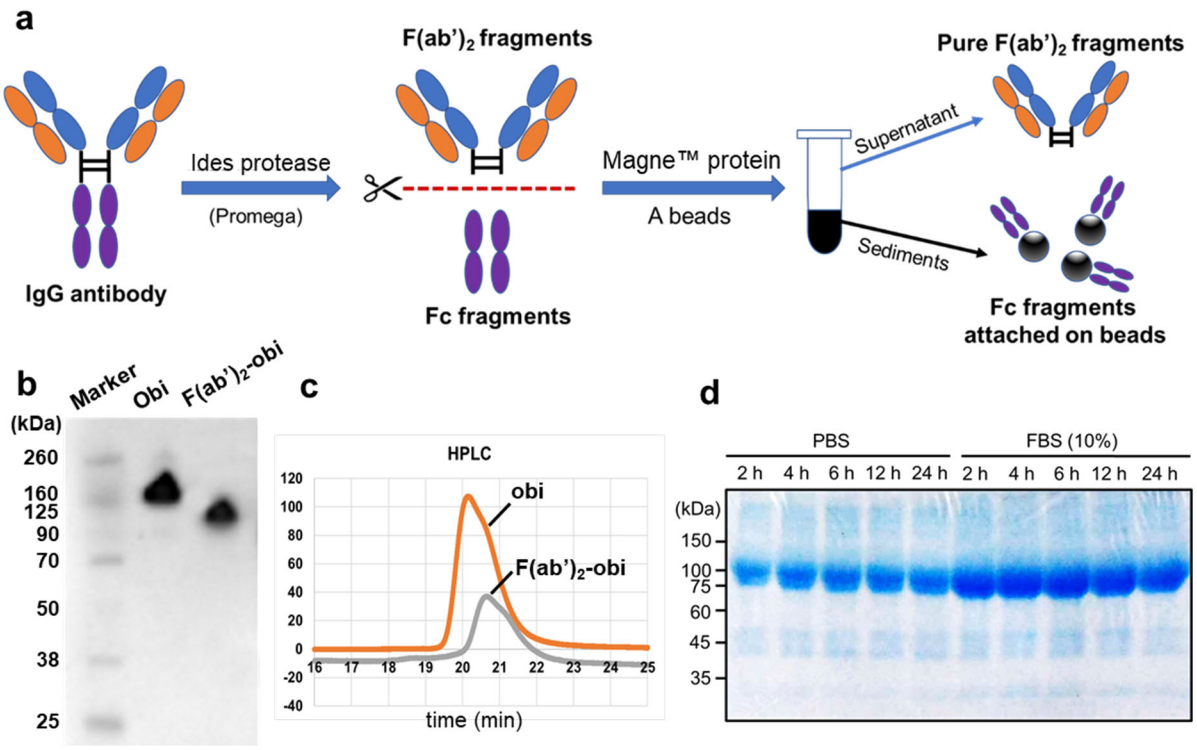

Figure 1. Preparation and verification of F(ab')$_2$. **(a)** F(ab')$_2$ fragments were prepared using IdeS protease and purified using magnetic protein A beads. **(b)** SDS-PAGE showed the size of obinutuzumab (obi) and F(ab')$_2$-obi. **(c)** HPLC showed the peak of F(ab')$_2$-obi right after its intact form. (d) SDS-PAGE displayed the good stability of F(ab')$_2$-obi after incubated in PBS or 10% FBS over 24 h.

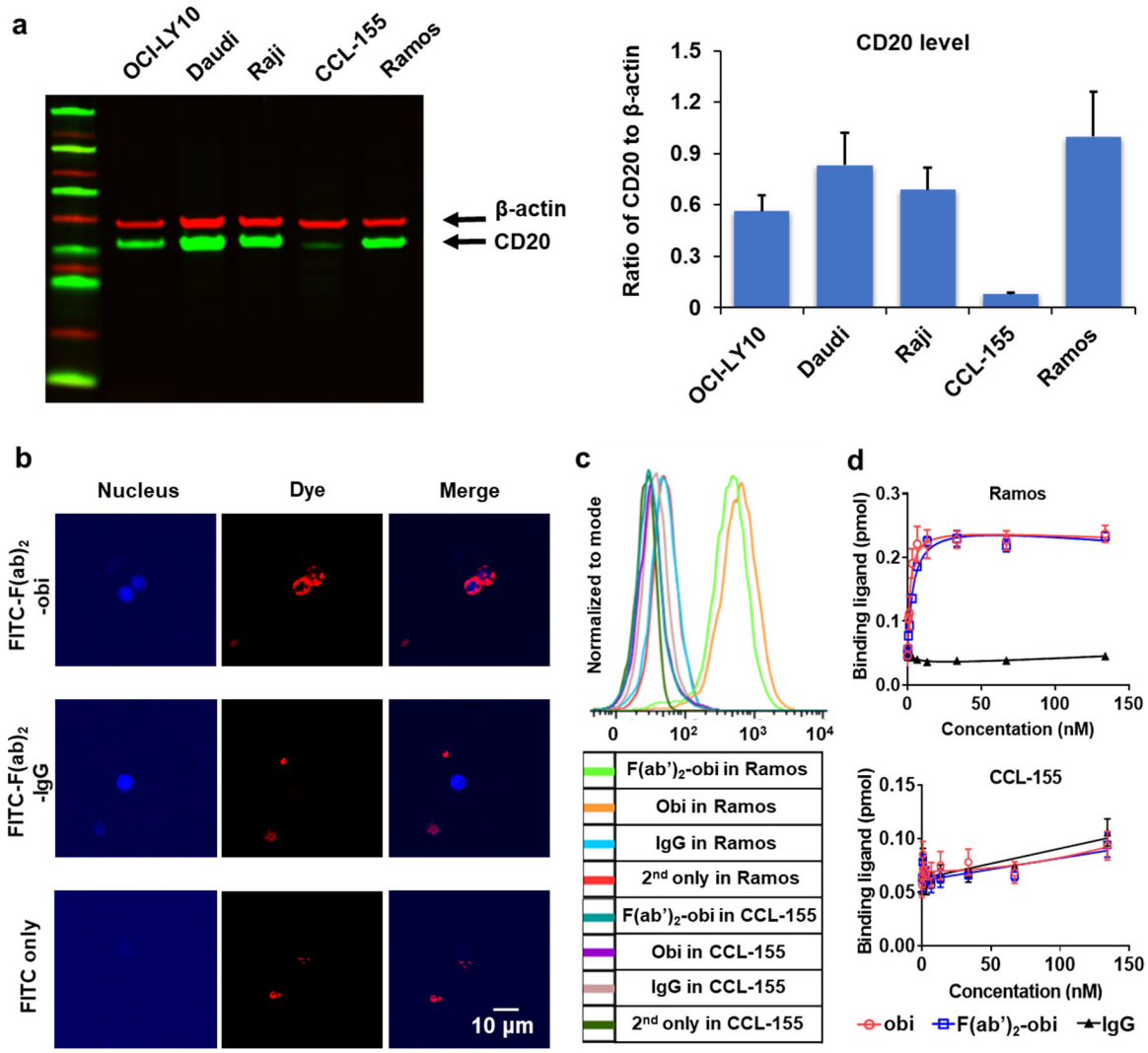

Figure 2. Cellular evaluation of CD20 expression and binding affinity. **(a)** Western blot showed CD20 expression of five different lymphoma cells **(b)** Confocal microscopy showed strong binding of F(ab')$_2$-obi with Ramos cells but not control samples. **(c)** Flow cytometry confirmed the specific binding of F(ab')$_2$-obi and obi with Ramos cells. (d) ELISA assay indicated that F(ab')$_2$-obi had high binding affinity with Ramos cells (K_D = 3.7 ± 0.6 nM, B_{max} = 0.22 ± 0.01 pmol).

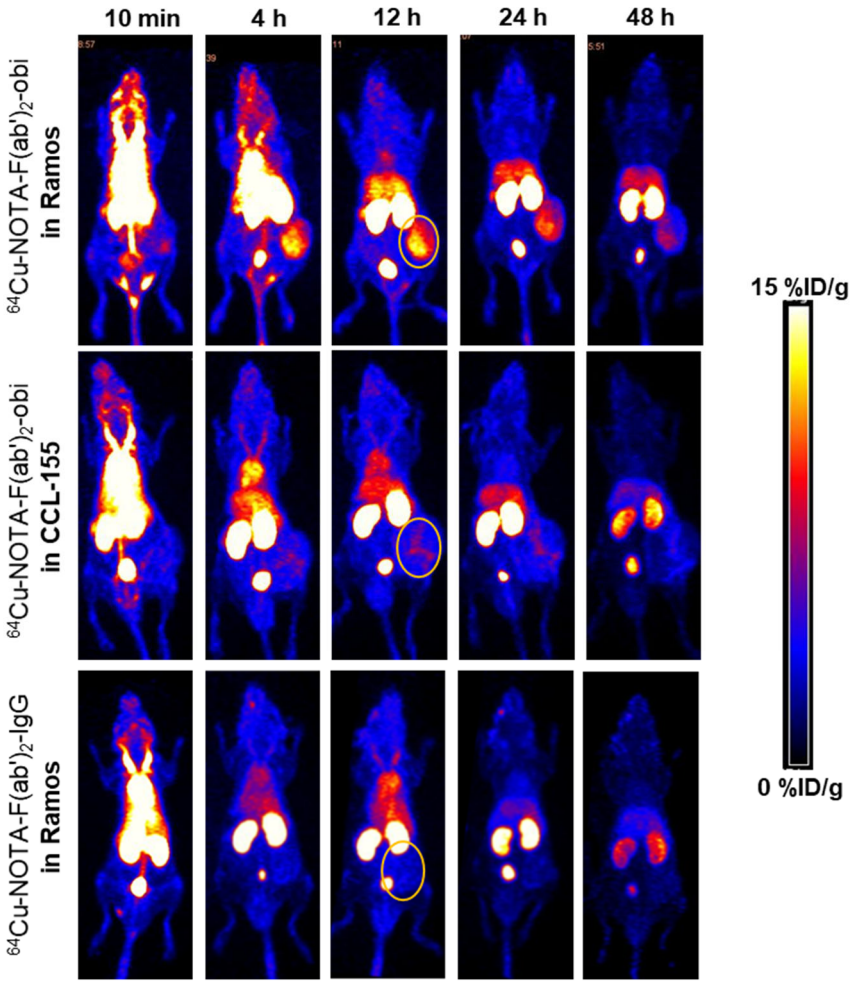

Figure 3. PET imaging of ^{64}Cu-NOTA-F(ab')$_2$-obi and ^{64}Cu-NOTA-F(ab')$_2$-IgG in Ramos and CCL-155 murine models. ^{64}Cu-NOTA-F(ab')$_2$-obi could visualize the Ramos tumor clearly after 4 h p.i. In contrast, ^{64}Cu-NOTA-F(ab')$_2$-IgG barely delineated the tumor. Besides, CCL-155 tumor could not be shown p.i. of ^{64}Cu-NOTA-F(ab')$_2$-obi. Circles indicated the tumors.

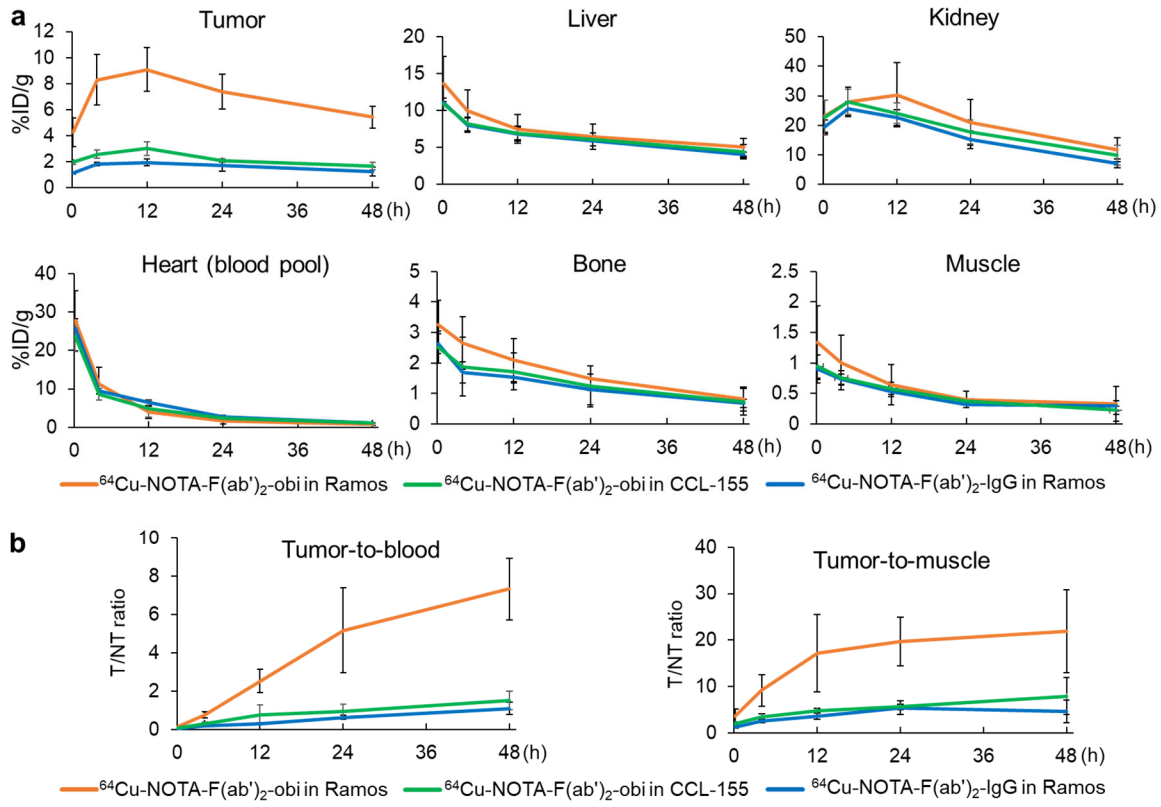

Figure 4. Semi-quantitative analysis of PET images. **(a)** Peak tumor uptake (9.1±1.7 %ID/g) was obtained at 12 h p.i. of ^{64}Cu-NOTA-F(ab')$_2$-obi in Ramos, which was significantly higher than F(ab')$_2$-IgG in Ramos (2.8±0.6 %ID/g) and F(ab')$_2$-obi in CCL-155 (1.9±0.3 %ID/g, P<0.001). **(b)** The tumor-to-blood (T/B) and tumor-o-muscle (T/M) ratios of ^{64}Cu-NOTA-F(ab')$_2$-obi in Ramos were significantly higher than those of control groups (P<0.05).

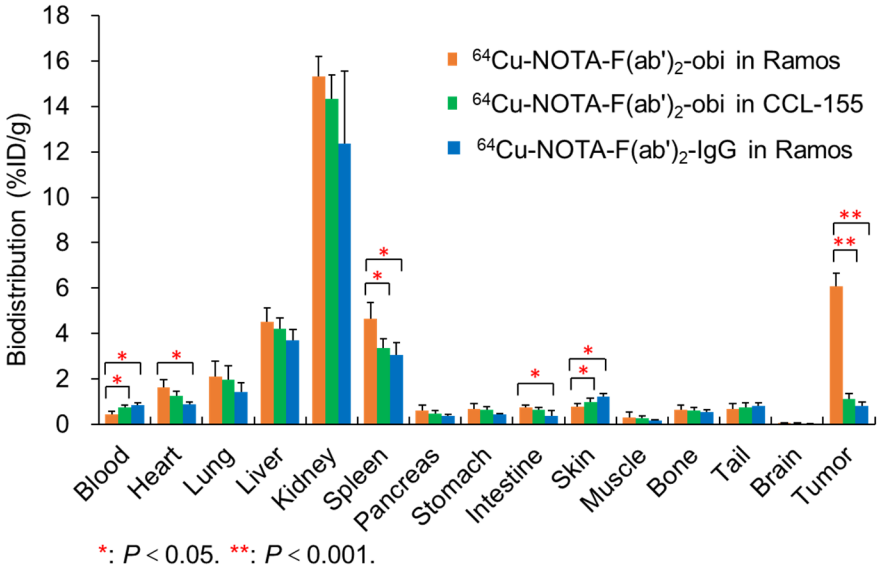

Figure 5. Biodistribution results at 48 h p.i. The tumor uptake of ^{64}Cu-NOTA-F(ab')$_2$-obi in Ramos was significantly higher than ^{64}Cu-NOTA-F(ab')$_2$-IgG in Ramos and ^{64}Cu-NOTA-F(ab')$_2$-obi in CCL-155 ($P < 0.001$). The renal uptake was higher than other organs in three groups while the blood uptake was all below 1 %ID/g. * : $P < 0.05$. **: $P < 0.001$.

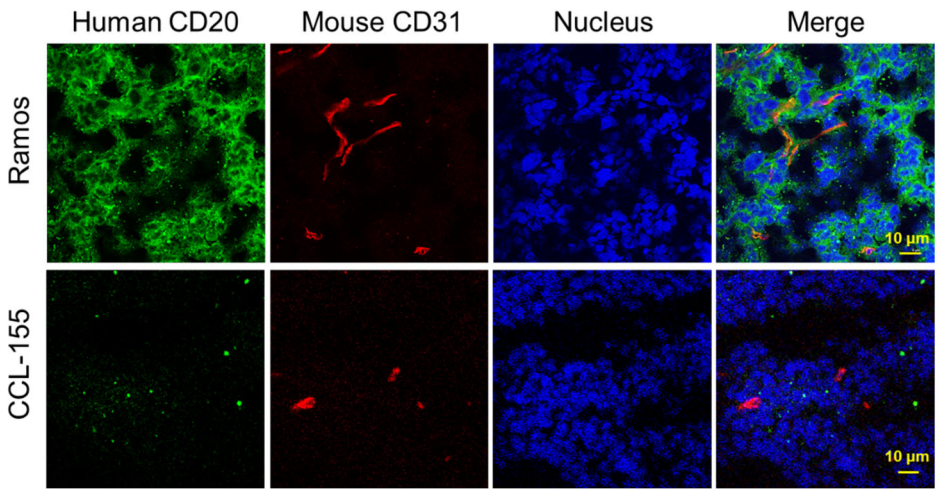

Figure 6. Immunofluorescence staining of tumor tissues. Strong CD20 expression (green signals) were found throughout Ramos tumors, while near-background signals were shown around CCL-155 tumors. CD31 signals represented angiogenesis. Scale bar = 10 μm.